Clock Duty Cycle Tuning for Desense Mitigation in Modulation -involved Cases

Shengxuan Xia¹, Jun Fan², Chulsoon Hwang³ EMC Laboratory, Missouri University of Science and Technology, Rolla, MO, USA
¹sx7c3, ²jfan, ³hwangc@mst.edu

Abstract—Nowadays consumers' electronic devices are highly integrated, and modules and integrated circuits (ICs) are usually placed close to each other due to the compact size. The modules and ICs may interfere with the radio frequency (RF) antennas and cause desense issues. In recent years, desense caused by direct coupling from the noise sources to the victim RF antennas has been well studied. However, more complicated mechanisms such as modulations between transmitting signals and low-frequency clock or data signals can also result in desense problems, especially in frequency divide duplex (FDD) applications. Typical solutions to desense problems will focus on suppressing the noise sources and/or the coupling paths, and little studies have shown the feasibility that desense in FDD applications can also be mitigated by engineering the spectral power distribution over the frequency range. This paper provides a comprehensive study on how to mitigate desense with the change in the spectrum distribution by tuning the duty cycle of the interfering clock. Measurements conducted on a real cellphone showed a 10 dB suppression of desense for certain TX bandwidth condition.

Keywords— desense, RF interference, clock, duty cycle, FDD, modulation.

I. INTRODUCTION

Radio frequency (RF) antenna desensitization problems, also known as desense, have drawn more attention in recent years. Due to the trend that modern electronic devices are designed to be more compact, equipped with more functions, and working under higher speed, unwanted noise sources and the coupling to the victim RF antennas will occur more frequently. There are many mechanisms that desense can happen on the RF antennas such as direct coupling [1][2], modulation [3], intermodulation [4][5], etc.

The most common cases are the direct coupling to the victim antennas. When there exist certain noise sources radiating frequency components within the receiving band, the antenna may pick up the noise when the sources have efficient coupling paths to it. Because the working frequency ranges of the antennas are known, it has been extensively studied to avoid unwanted noise coupled to the antenna from nearby modules. Typical mitigation solutions include shielding, absorbers, and even rotating the orientation [1]. The reciprocity-based theorem is used as a framework to model the direct coupling problem [6]. Based on the framework, several methods have been proposed such as equivalent dipole moment extraction for noise source modeling [7][8] or using Huygens box [9].

Desense problems with modulation involved are more difficult to identify. The radiating transmitting signals can be as high as 23 dBm, and a significant amount of TX power can be easily coupled to nearby modules and components. Owing to the nonlinearity of the components, coupled TX signals modulated with low-frequency baseband signals generate new frequency components and then interfere with the RX band. The low-frequency baseband signals, which are typically ignored for the desense issues, can be troublemakers in such situation. There exist little study on relationship between the baseband signal spectrum and desense.

In this paper, a new direction for desense mitigation is proposed. Without modifying the hardware design, desense can be suppressed by engineering the spectrum distribution through tuning the noise clock duty cycle. The understandings of modulation caused desense and the clock spectrum distribution versus duty cycle are explained. Then the real cellphone measurements validated the feasibility of desense mitigation by the tuning of duty cycle.

II. MODULATION INVOLVED DESENSE ISSUES

A. Brief Introduction to the Modulation Casused Desense

For frequency divide duplex (FDD) working mode RF antennas, the transmitting frequencies are usually not far away from the receiving frequency range. As. Fig. 1 (a) shows, using LTE band 5 as an example, the transmitting channels have a 45 MHz difference to the receiving channels. Modulation-caused desense can happen under two conditions: 1) There exist baseband signal spectral components around 45 MHz; 2) There is sufficient nonlinearity to mix the TX and the baseband signals. Then the baseband signals will be up-converted into the RX range and interfere with the channel. Previous study has well identified this modulation mechanism happened in a practical phone design [3].

As Fig. 1 (b) shows, the TX signals radiated from the antenna can be picked up by the nearby digital microphone (Dmic) circuit. Due to the nonlinearity of the Dmic component, the coupled TX signals, can modulate with the clock signals on the mic, thus, new unwanted high-frequency signals at the RX range will be created after the mixing. Eventually, the modulated RX noise will couple back to the victim antenna and degrade the sensitivity. Notice that although the Dmic clock's fundamental frequency is 2.4 MHz, its harmonics can occur near 45 MHz.

Therefore, the interfering signals come from the intermodulation between TX and its harmonics of the Dmic clock.

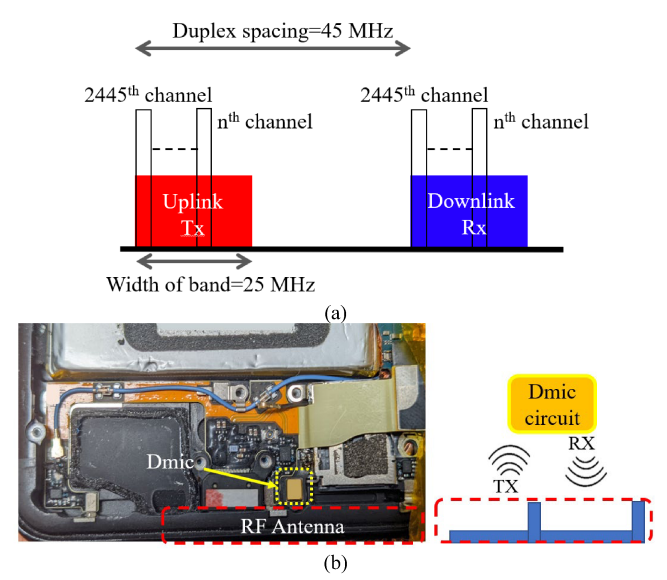


Fig. 1. Modulation caused desense mechanism: (a) FDD mode working band (b5); (b) round-trip coupling of TX and modulated clock signals.

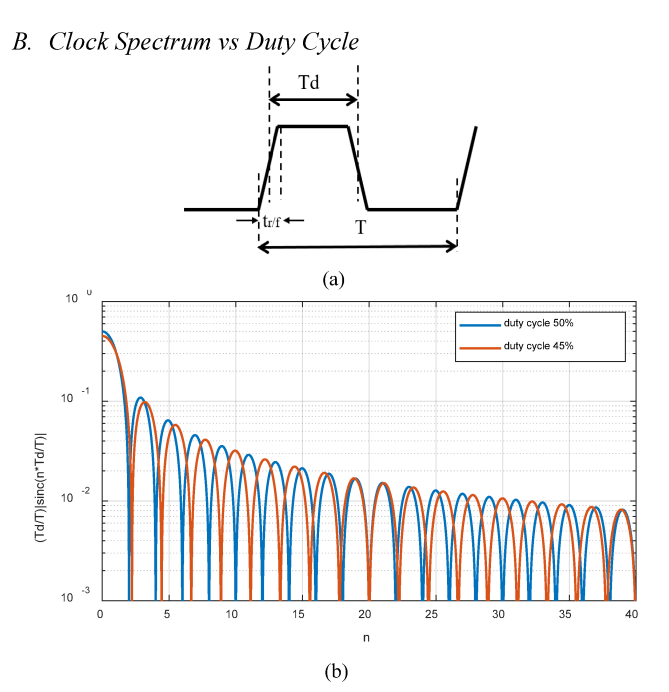


Fig. 2. Trapezoidal wave and the sinc function for different duty cycles: (a) Explanations of trapezoidal wave; (b) sinc function over harmonic orders.

A clock can be reasonably treated as a trapezoidal wave with a certain rise/fall time and duty cycle as Fig. 2 (a) shows. The waveform can be expressed in the Fourier series as [10]:

$$x(t) = c_0 + \sum_{n=1}^{\infty} 2c_n \cos(n\omega_0 t + \theta_n)$$
 (1)

where x(t) is the time domain waveform of the trapezoidal wave, c_0 is the DC component, and c_n is double-sided spectrum amplitude of the n^{th} order harmonic. Applying Fourier transform, the magnitudes of the single-sided Fourier coefficients (exclude DC) of the clock harmonics can be expressed as:

$$c_n^{+} = 2c_n = 2A\frac{T_d}{T} \left| \frac{\sin\left(\frac{n\pi T_d}{T}\right)}{\frac{n\pi T_d}{T}} \right| \frac{\sin\left(\frac{n\pi t_{r/f}}{T}\right)}{\frac{n\pi t_{r/f}}{T}}$$
(2)

where c_n^+ is the single-sided Fourier coefficient for nth order harmonic, A is the amplitude of voltage level for digital "HIGH", T_d is the on-time pulse width, T is the period, $t_{r/f}$ is the rise/fall time. It is well known that the duty cycle is usually close to 50%, and the trapezoidal wave will only have odd order harmonics to be dominant while all even harmonics are practically negligible. However, this is not valid for higher order harmonics.

Assuming the rise/fall time, period, and the voltage amplitude are all fixed and only the duty cycle changes, the Fourier coefficients, Y(n), become to

$$Y(n) = (T_d/T) \left| \sin(n\pi T_d/T) / (n\pi T_d/T) \right| \tag{3}$$

which is only related to the duty cycle. Fig. 2 (b) shows the coefficients for different duty cycles. For example, for 50% duty cycle case, Y(n) is zero when n=10 (even order) and non-zero when n=9 (odd order). However, when the duty cycle is not ideal, for example 45% case, $Y(n=9) \ll Y(n=10)$. In this case, even order component is much greater than odd order component. It is worth mention that, from Fig. 2 (b), that the dominance between odd and even order harmonics alternates as the frequencies increase.

C. Interfering Clock Harmonics for Different TX Bandwidth

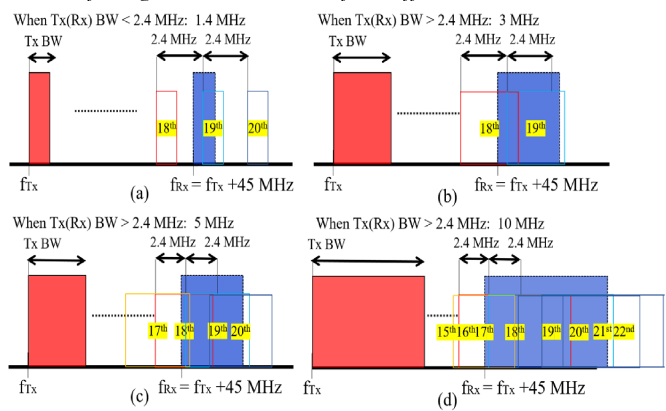


Fig. 3. Interfering clock harmonic orders for different TX bandwidth: (a) 1.4MHz; (b) 3MHz; (c) 5MHz; (d) 10MHz.

The clock harmonics are narrow-band signals, but the TX signals are wide-band. The up-converted sideband noise due to the modulation will be wideband, and the bandwidth of each modulated harmonic will be equal to that of TX. The simplest case is shown in Fig. 3 (a) when the TX bandwidth is smaller than the fundamental frequency of the Dmic clock. Only partial

power of the 19th order of the harmonic will interfere with the receiving band. When it comes to the cases with wider TX bandwidth, the 19th order harmonic will always interfere with the RX band while more and more adjacent harmonics will be involved as the TX/RX bandwidth increases. As. Fig. 3(b) (c) (d) demonstrate, when TX/RX bandwidth is 3 MHz, 18th and 19th harmonics will partially contribute to the total received power, known as received signal strength indicator (RSSI), within the RX range. While when TX/RX bandwidth is 5 MHz, 17th ~20th harmonics will interfere with the RSSI and when TX/RX bandwidth is 10 MHz, the 15th ~22nd harmonics contribute to RSSI. As mentioned in Section II Part A, regardless of channels selected to transmit and receive, the duplex spacing always keeps the same. But when the TX bandwidth becomes wider (indicated as the red blocks), the modulated harmonics will also be wider. Then more harmonics will fall into the receiving band (indicated as the blue blocks). Also, each order will have a different contribution weight to the RSSI.

As Fig. 4 shows, the measured wideband TX signal occupies a 1.4 MHz bandwidth and the RF power will be dominant within the frequency range of $[f_{TX}, f_{TX} + Bandwidth_{TX/RX}]$, in this example $Bandwidth_{TX/RX} = 1.4$ MHz. Furthermore, only part of the modulated 19th harmonic will interfere with the receiving range as Fig. 3 (a) shows, so the accordingly considered frequency range is marked in Fig. 4 (a) shadowed range. Then the unwanted power at the nth order harmonic can be expressed as [11]:

$$P\left(n, \frac{T_d}{T}\right) = \alpha \cdot c_n^+ \left(n, \frac{T_d}{T}\right) \cdot 2 \int_{f=f_1(n)}^{f=f_2(n)} S_{xx}(f) df$$
 (4)

where $\frac{T_d}{T}$ is the duty cycle, $f_1(n)$ and $f_2(n)$ are the lower and upper boundaries of nth order harmonic for considered frequency range within $[f_{TX}, f_{TX} + Bandwidth_{TX/RX}]$, $S_{xx}(f)$ is the spectral density of the TX signal. The coefficient α is a constant representing the round-trip EM coupling efficiency and the mixing conversion loss between TX and clock harmonics. In other words, the integrated total TX power within the given frequency band will be firstly coupled from the antenna to the Dmic, then modulated with clock harmonics, and eventually couple back to the antenna. Unless the coupling path and the nonlinearity of the Dmic change, α remains unchanged. Also, because the duplex spacing is much smaller than the carrier frequencies, the frequency dependency of α can be neglected.

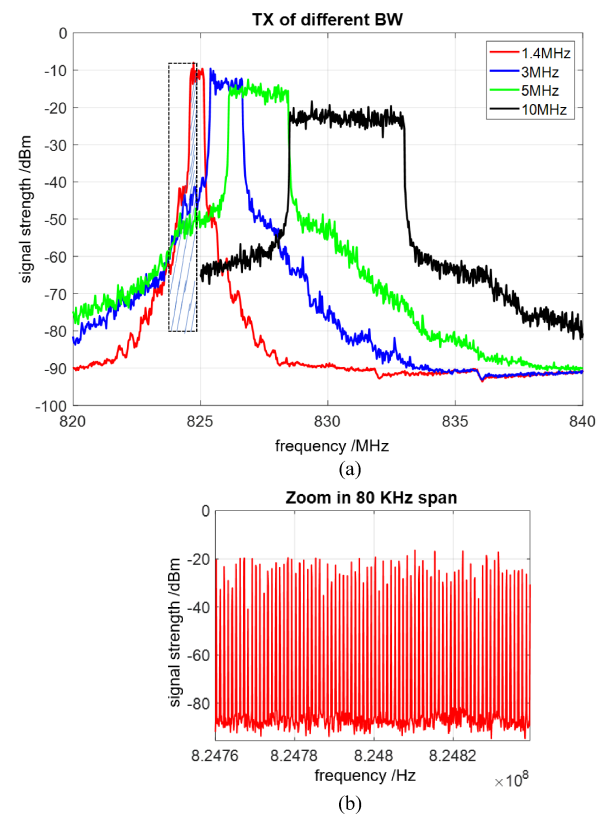


Fig. 4. TX spectrum and the interfering RF power: (a) TX signals (different bandwidth settings) (b) zoomed in spectrum of TX (10MHz case).

Furthermore, the wideband TX signal is not a continuous spectrum but is composed of thousands of narrowband tones with 1 KHz interval between adjacent tones if zoomed in to a small span as Fig. 4 (b) shows. When the resolution bandwidth (RBW) is much smaller than 1 KHz, the integral in (4) can be simplified as a summation:

$$P\left(n, \frac{T_d}{T}\right) = \alpha \cdot c_n^+ \left(n, \frac{T_d}{T}\right) \cdot \sum_{m=m_i}^{m=m_2} P_{measured}\left(m\right)$$
 (5)

where $P_{measured}$ is the measured curve in the spectrum analyzer. m_1 and m_2 satisfy $f(m_1) = f_1$ and $f(m_2) = f_2$. f(m) is the recorded frequency axis data. As it can be observed in Fig. 4 (a), the spectrum distributions over frequencies of the TX are roughly flat within the working bandwidth. Therefore, if the total radiation TX power is known, (5) can be further simplified as:

$$P\left(n, \frac{T_d}{T}\right) \approx \alpha \cdot c_n^+ \left(n, \frac{T_d}{T}\right) \cdot P_{TX} \cdot w(n)$$
 (6)

$$w(n) = \frac{\left| f_2(n) - f_1(n) \right|}{Bandwidth_{TX/RX}}$$
 (7)

$$RSSI\left(\frac{T_d}{T}\right) = P_{RX}\left(\frac{T_d}{T}\right) = \sum_{n} P\left(n, \frac{T_d}{T}\right)$$
 (8)

where P_{TX} is the total power of TX, w(n) is the weighting coefficients to represent the ratio of the involved power to the total power for n^{th} order harmonic.

TABLE I. WEIGHTING COEFFICIENTS FOR INVOLVED HARMONICS

TX/RX bandwidth	1.4 MHz	3 MHz	5 MHz	10 MHz
w(n)	$w(19) = \frac{0.8}{1.4}$	$w(18) = \frac{1.2}{3}$ $w(19) = \frac{2.4}{3}$	$w(17) = \frac{0.8}{5}$ $w(18) = \frac{3.2}{5}$ $w(19) = \frac{4.4}{5}$ $w(20) = \frac{2}{5}$	$w(15) = \frac{1}{10}, w(16) = \frac{3.4}{10}$ $w(17) = \frac{5.8}{10}, w(18) = \frac{8.2}{10}$ $w(19) = \frac{9.4}{10}, w(20) = \frac{7}{10}$ $w(21) = \frac{4.6}{10}, w(22) = \frac{2.2}{10}$

As the RSSI caused by TX & harmonics modulation is related to specific order(s) of the harmonics, and each harmonic has a different contribution weight to the desense level, RSSI will be determined by the summation of all the involved harmonics' power multiply by their weights. When the amplitudes of several adjacent harmonics can be tuned according to (2), there may exist an optimal option to have the RSSI minimized.

III. DESENSE MITIGATION MEASUREMENT VALIDATIONS

According to the derivations in (4)~(8), the interfering RF power is a function of the duty cycle. Tuning the duty cycle will result in varying c_n^+ and thus varying RSSI. To validate the feasibility of desense mitigation, two measurements were conducted. Considering practical limitation that the Dmic inside the phone cannot modify the clock duty cycle, a separate Dmic module was used and powered up by an adjustable external signal generator. The Dmic module was placed nearby the cellphone RF antenna to maintain the coupling path as Fig. 5 shows. The Dmic was provided with the clock signal and DC bias from a function generator (Agilent 81150A). In this setup, the round-trip coupling and the up-conversion due to nonlinearity still exist to mimic the same mechanism as Fig.1 (b).

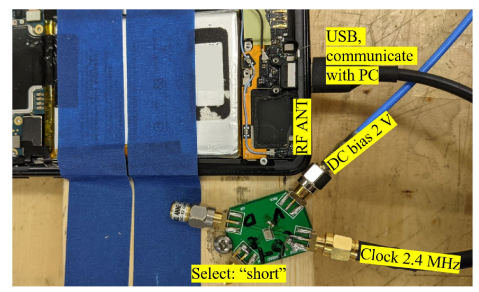


Fig. 5. Cellphone RFI setup for TX & clock modulation caused desense

A. Duplexer-based Cellphone RFI Test

To better observe the RX spectrum changes as a function of the duty cycle, an LTE band 5 supported duplexer was used to enable access to the received spectrum. While maintaining the placement of the cellphone and the Dmic module, the wirings were changed as shown in Fig. 6 (a). Fig. 6 (b) depicts the wiring diagram and the RF signal paths. The high-power phone TX signals first went through the "TX" port to the "ANT" port of the duplexer and then injected into the RF antenna system (tuning circuits + physical antenna). The radiated TX signals were coupled to the Dmic and modulated with the clock harmonics. Then the modulated sideband is radiated back and picked up by the antenna. Eventually, the picked RX sideband signals went through the "ANT" port to the "RX" port of the

duplexer and got measured by the spectrum analyzer (amplified before going into the instrument).

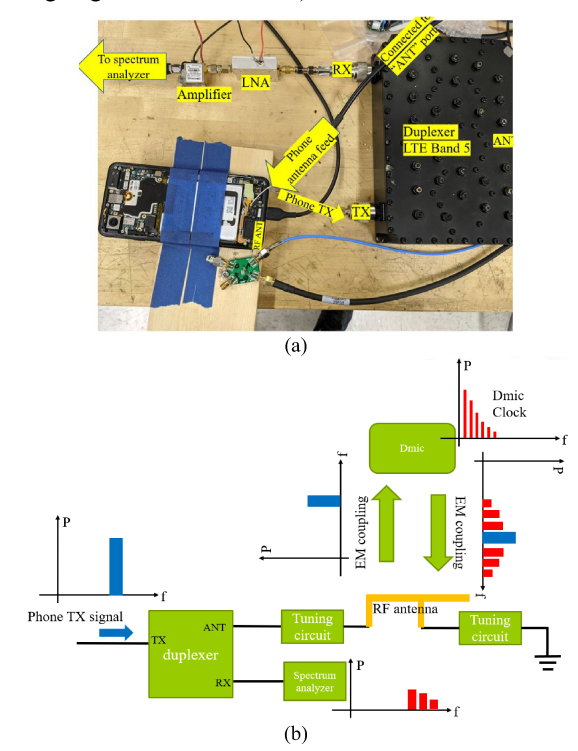


Fig. 6. Duplexer-based RFI test setup: (a) actual setup; (b) wiring diagram and signal flow paths.

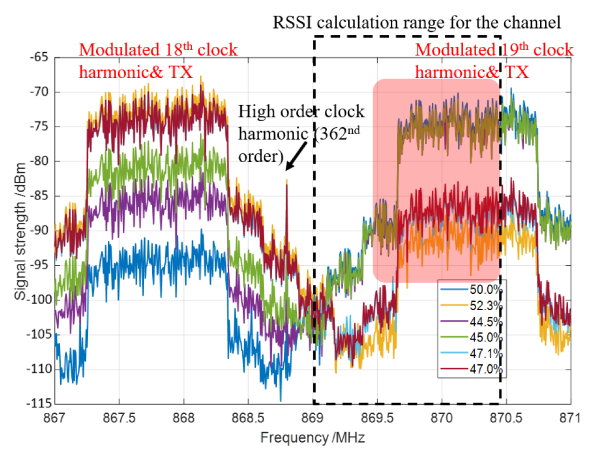


Fig. 7. Duplexer-based RFI test results

The measured results are shown in Fig. 7 for the case that the TX bandwidth is 1.4MHz. As discussed in Section II Part C, the interfering frequency range of the 19th harmonic is marked as the transparent red region. By changing the clock duty cycle, more than 10dB difference can be seen in the marked range.

B. Measured RSSI in Real Phones

When it comes to wider TX bandwidth cases, the spectrum in the RX range will be more complicated because of the overlapping of the modulated harmonics. Thus, measuring the spectrums for wider TX cases becomes unnecessary. Therefore,

direct RSSI tests can help to find out the optimal duty cycle setting for desense mitigation for all TX/RX bandwidth settings. There is a commercial tool installed on a PC that can control and communicate with the phone under test. Real-time RSSI can be directly recorded on the PC. Measurements were done for 3 different TX bandwidth settings and a sweeping of duty cycle from 46% to 54% with the resolution of 0.1% (finest resolution of the signal generator). Equation-based RSSI change predictions will be given by (7).

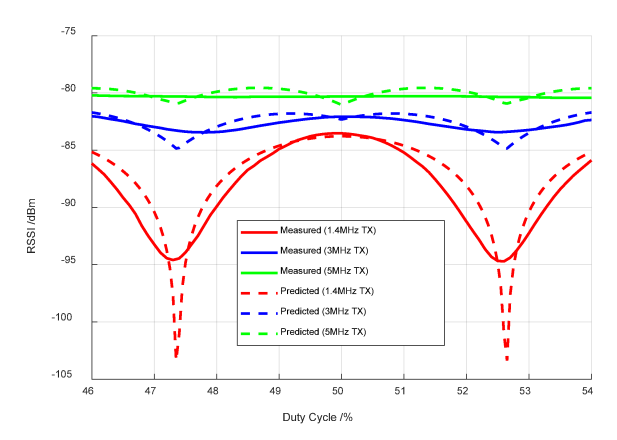


Fig. 8. Direct RSSI test results

The trends of desense level, as shown in Fig. 8, changed for different bandwidths are well captured. The smaller bandwidth, the higher suppression on desense can be achieved using this clock-duty tuning method. Ideally, if the modulated clock harmonics are the only noise sources, and the duty cycle can be tuned with 0.05% resolution as the dashed red curve shows, desense can be mitigated by 20 dB (47.35% or 52.65%) for the 1.4 MHz bandwidth case. However, due to the existence of other small noises and the limitation of the signal generator's finest tuning capability, a 10 dB mitigation is the best improvement. For the 5 MHz bandwidth case, the actual measurement won't be able to resolve such a small difference of 1.5 dB.

IV. CONCLUSIONS

This paper demonstrates a comprehensive understanding of how the modulated harmonics will undermine the receiving sensitivity in an FDD mode RF system. Based on the understandings, a new direction that changing the spectrum envelope by tuning the noise source clock duty cycle is proposed to mitigate desense for the first time. Equation-based estimations have been derived and well validated with the real product measurements. When the interfering clock signals do not require

a strict duty cycle to function properly, this tuning method can be used to suppress desense without any modifications on the layout design. Therefore, in the future, the modulation-involved desense problems can be solved in a new applicable method for engineers.

REFERENCES

- C. Hwang and Q. Huang, "IC placement optimization for RF interference based on dipole moment sources and reciprocity," *IEEE Asia-Pacific Electromagn. Compat. Symp.*, 2017, pp.331-333.
- [2] Y. Sun, H. Lin, B.C. Tseng, D. Pommerenke and C. Hwang, "Mechanism and Validation of USB 3.0 Connector Caused Radio Frequency Interference," *IEEE Trans. Electromagn. Compat.*, Jul. 2019.
- [3] S. Xia, et al., " RFI Estimation for Multiple Noise Sources Due to Modulation at a Digital Mic Using Diople Moment Based Reciprocity," 2020 IEEE International Symposium on Electromagnetic Compatibility & Signal/Power Integrity (EMCSI), 2020, pp. 1-5, doi: 10.1109/EMCSI38923.2020.9743517.
- [4] J. Li et al., "Self-contact Introduced Passive Intermodulation Characterizations for Captured Springs," 2021 IEEE International Joint EMC/SI/PI and EMC Europe Symposium, 2021, pp. 929-934, doi: 10.1109/EMC/SI/PI/EMCEurope52599.2021.9559265.
- [5] S. Xia et al., "Gaussian Process Regression Analysis of Passive Intermodulation Level and DCR for Spring Contacts," 2021 IEEE International Joint EMC/SI/PI and EMC Europe Symposium, 2021, pp. 935-939, doi: 10.1109/EMC/SI/PI/EMCEurope52599.2021.9559359.
- [6] J. Pan, H. Wang, X. Gao, C. Hwang, E. Song, H.-B. Park, and J. Fan, "Radio-Frequency Interference Estimation Using Equivalent Dipole moment Models and Decomposition Method Based on Reciprocity," *IEEE Transactions on Electromagnetic Compatibility*, vol. 58, no. 1, pp. 75–84, 2016.
- [7] Q. Huang, Y. Liu, L. Li, Y. Wang, C. Wu, and J. Fan, "Radio frequency interference estimation using transfer function based dipole moment model," 2018 IEEE International Symposium on Electromagnetic Compatibility and 2018 IEEE Asia-Pacific Symposium on Electromagnetic Compatibility (EMC/APEMC), 2018.
- [8] Q. Huang, F. Zhang, T. Enomoto, J. Maeshima, K. Araki and C. Hwang, "Physics-based dipole moment source reconstruction for RFI on a practical cellphone", *IEEE Trans. Electromagn. Compat.*, vol. 59, no. 6, pp. 1693-1700, Dec. 2017.
- [9] Y. Sun, B.C. Tseng, H. Lin, and C. Hwang, "RFI Noise Source Quantification Based on Reciprocity," in *Proc. IEEE Int. Symp. Electromagn. Compat.*, Jul. 2018, pp. 548-553.
- [10] D. Su, K. Zhu, M. Niu and X. Wang, "A quantified method for characterizing harmonic components from EMI spectrum," 2015 AsiaPacific Symposium on Electromagnetic Compatibility (APEMC), Taipei, 2015, pp. 561-564.
- [11] Howard, R. M. (2004). Principles of Random Signal Analysis and low noise design: The Power Spectral Density and its applications. Wiley.